Tracking nanoplastics in drinking water: a new frontier with the combination of dielectrophoresis and Raman spectroscopy

Microplastics and Nanoplastics

RESEARCH

Open Access

Tracking nanoplastics in drinking water: a new frontier with the combination of dielectrophoresis and Raman spectroscopy

Marta Fadda[1], Alessio Sacco[1], Korinna Altmann[2], Dmitri Ciornii[2], Frank Milczewski[2], Miguel A. Bañares[3], Raquel Portela[3], Andrea Mario Giovannozzi[1*] and Andrea Mario Rossi[1]

Abstract

Detection of micro- (MPs) and nanoplastics (NPs) in food and environmental matrices has been gaining relevance due to their potential toxicological effects on human health. While MPs have been detected in a wide range of complex matrices, suitable methods for the characterization and chemical identification of NPs are still lacking, primarily due to significant methodological challenges associated with their nano-specific physiochemical properties, including size distribution (1 nm – 1 µm), dynamic surface chemical changes, and carbon-based composition, which complicate their detection compared to engineered nanomaterials. To overcome the traditional limitations of spectroscopic techniques in terms of spatial resolution and sensitivity at the sub-micrometer level, a novel label-free methodology is presented for specifically identifying the chemical composition of NPs directly in suspension by combining Raman spectroscopy with dielectrophoresis (DEP). Using a custom-built device, small volumes of NPs are injected into a dielectrophoretic cell and locally trapped by DEP forces to fill the Raman confocal volume, facilitating their detection and identification, and providing high signal-to-noise ratio Raman spectra for more reliable analysis. This approach was successfully applied to both Milli-Q water and a commercial brand of drinking water, enabling the rapid identification of various types of NPs with different sizes and polymer compositions at concentrations as low as 20 µg/mL. These included certified reference polystyrene beads ranging from 800 to 60 nm in diameter, as well as polydisperse NPs, more representative of real samples in terms of size distribution and polymer type, such as polyethylene (450 nm), polypropylene (180 nm), and polyethylene terephthalate (100 nm). Moreover, the chemical fingerprint of each NPs was thoroughly investigated and compared with the corresponding bulk polymers, highlighting possible changes in the Raman bands due to surface oxidation or nanometer-scale effect. Therefore, this innovative method can be considered a valuable approach for addressing gaps in the detection and identification of NPs, as well as for monitoring their dynamic phisiochemical changes in real matrices.

Keywords Microplastics, Nanoplastics, Drinking water, Raman spectroscopy, Dielectrophoresis

Introduction

Nowadays, microplastics (MPs) and nanoplastics (NPs) are considered a major issue, not only for the environment, but also for human health [1–3]. When plastic waste is not properly disposed and, thus released into the environment, it can break down into smaller fragments — MPs (1 µm to 1 mm, ISO/TR 21960:2020 [4]) and NPs (1 nm to 1 µm, ISO/TR 21960:2020 [4]) — through processes such as photo-thermal degradation, chemical

*Correspondence:
Andrea Mario Giovannozzi
a.giovannozzi@inrim.it
[1] Quantum Metrology and Nano Technologies Division, Istituto Nazionale Di Ricerca Metrologica (INRiM), Turin 10135, Italy
[2] Bundesanstalt Für Materialforschung Und-Prüfung (BAM), Berlin 12205, Germany
[3] Consejo Superior de Investigaciones Científicas-Institute of Catalysis and Petrochemistry (CSIC-ICP), Madrid 28049, Spain

decomposition by hydrolysis, oxidation and mechanical abrasion, eventually entering the food chain [5]. Since the most common thermoplastic polymers (e.g. polyethylene terephthalate (PET), polypropylene (PP), polyethylene (PE), polystyrene (PS), poly(methyl methacrylate) (PMMA)) have low degradability and long-life in the environment, the continued accumulation of MPs and NPs in environmental compartments and their potential impacts on biota and human health has emerged as an urgent planetary problem [6–9]. Although it is well known that plastic particles smaller than 10 μm can be inhaled [10], as well as those smaller than 1 μm can go through the intestinal barrier [11], their negative impact has to be clarified yet, mainly because representative reference materials and standardized analytical methods, particularly for NPs, are still lacking. This is primarily due to significant methodological challenges associated with their nano-specific physiochemical properties, including size distribution (1 nm – 1 μm), dynamic surface chemical changes (e.g. release of chemicals, surface oxidation), and carbon-based composition, which makes their proper detection and identification significantly more difficult compared to engineered nanomaterials [7]. Furthermore, nearly all previous studies on NPs have been based on commercially available PS particles that are monodispersed, spherical, stabilized with surfactants and/or doped with metals [12, 13]. In contrast, "environmental" NPs are polydisperse and have irregular shapes, and hence truly representative test/reference materials should be used for more realistic analytical applications [14]. To date, a variety of orthogonal measurement techniques have been employed and evaluated for a comprehensive physicochemical characterization of NPs. These included dynamic light scattering, nanoparticle tracking analysis, tunable resistive pulse sensing, transmission and scanning electron microscopy, as well as separation/fractionation methods such as centrifugal liquid sedimentation, and field-flow fractionation–multi-angle light scattering combined with pyrolysis gas chromatography mass spectrometry, or Raman microspectroscopy, for the determination of NPs size, shape, chemical composition and for quantification [15]. Although the techniques outlined above have the potential (alone or in combination) for the detection and characterization of NPs, only a few are truly established, and several limitations are still present. Regarding chemical identification, Raman microspectroscopy has become a well-established technique for MP analysis, as it enables specific chemical characterization of polymers alongside size distribution analysis down to approximately 1 μm when coupled with a confocal microscope [7, 16]. Although, in theory, a spatial resolution of up to about 300 nm can be achieved, analyzing particles smaller than 500–1000 nm remains highly challenging [7]. To address these instrumental limitations in spatial resolution and sensitivity, various combinations with high-resolution techniques, or NPs trapping tools were proposed. For instance, correlative approaches combining Raman spectroscopy with SEM or SEM-energy dispersive X-ray (EDX) were reported to provide both high-resolution imaging and chemical identification of NPs [17, 18]. However, these methodologies present various technical limitations, such as complex sample preparation procedures, the difficulty in maintaining the correspondence of the NPs detected by electron microcopy during vibrational spectroscopy analysis, and the limited forms in which NPs can be analyzed. Alternatively, Raman spectroscopy combined with optical tweezers was proposed to trap NPs, thus filling the confocal volume to enhance sensitivity and enable analysis in-line with fractionation/light scattering techniques. Even though this method allows the identification of NPs in suspension, various limitations and open questions remain, mostly regarding the minimal concentration and size of NPs that can be detected. For instance, Schwaferts et al. reported a minimal concentration of 200 μg/mL for PS particles (200 nm), with no results provided for smaller NPs [19]. Gillibert et al. identified NPs by estimating the number of trapped particles, revealing a limit of applicability for particles down to 500 nm in diameter, and providing Raman spectra with low signal-to-noise ratio for agglomerates/aggregates of 20–30 PS NPs with a diameter of 90 nm and 50 nm [20]. Furthermore, surface enhanced Raman spectroscopy was also presented as innovative approach to identify NPs [21, 22], even though its limitations are mainly related to sample preparation procedure, as well as reproducibility, spectral perturbations that limit the spectra interpretation, mainly in complex matrices.

Here we propose a novel label-free methodology for specifically identifying the chemical composition of NPs directly in suspension by combining Raman spectroscopy with dielectrophoresis (DEP). DEP is a well-known phenomenon that allows the manipulation of dielectric and conducting particles via a non-uniform electric field. Commonly, this phenomenon has been used for several applications such as transportation, separation and accumulation of dielectric micro and nanoparticles, including bacteria, virus, microplastics and nanoplastics [23–26]. The dielectrophoretic force (FDEP) is expressed as [26]:

$$F_{DEP} = 2\pi r^3 \varepsilon_0 \varepsilon_m Re[f_{CM}] \nabla E_{rms}^2 \quad (1)$$

where r is the particle radius, ε0 is the permittivity of the vacuum, εm is the dielectric constant of the medium, fCM is a complex variable Clausius–Mossotti factor, and

Erms is the root-mean-square value of the applied electric field. The fCM describes the relative polarization of a particle and is defined as [26]:

$$f_{CM} = \frac{\varepsilon_p^* - \varepsilon_m^*}{\varepsilon_p^* + 2\varepsilon_m^*} \quad (2)$$

where $\varepsilon^* = \varepsilon_0\varepsilon - \frac{i\sigma}{\omega}$ is the complex permittivity of the particle (p subindex) or the medium (m subindex), in which σ is the electric conductivity, and ω is the angular frequency of the applied electric field. FDEP pushes the particles towards the region of strong electric field if the Re[fCM] > 0 (positive DEP), off this region if Re[fCM] < 0 (negative DEP) [26]. The application of DEP to MPs and NPs was previously investigated: for instance, Bu et al. studied theoretically and experimentally the AC-insulating DEP behaviors of PS beads with different diameters (980 nm and 280 nm) and surface functionalization (carboxylate and native PS) in various ionic mediums in a low-frequency regime, comparing their migration and trapping, hypothesizing its feasibility in identification and characterization of NPs [27]. In another study, Beech et al. experienced the separation of PS with diameter of 250 nm and 500 nm inside a device that combined deterministic lateral displacement, where particles crossed streamlines and followed different trajectories through the device due to their steric interaction with active posts, and DEP, which, together with steric interaction, forced the displacement mode [28]. Furthermore, DEP in combination with Raman spectroscopy has been already used for chemical identification of various species, such as plant pathogenic bacteria [29], or pathogens recovered from urinary tract [30], or suspended tungsten trioxide (WO3) and polystyrene nanoparticles to map their spatial concentration in a microfluidic dielectrophoresis platform [31], demonstrating its feasibility for chemical identification of suspended nanoparticles without further sample preparation. In this work, therefore, we combine DEP and Raman spectroscopy for trapping and identifying NPs of various sizes and polymer types, fulfilling an important gap in this field of application.

In this work, a new methodology is proposed for identifying NPs in aqueous suspensions with Raman spectroscopy enabled by DEP. DEP is used to accumulate NPs, increasing their local population density to fill the confocal volume of the Raman microscope, thereby overcoming spatial resolution limitations and optimizing the signal-to-noise ratio for Raman analysis of NPs-dispersed samples. The performance of this DEP-Raman system was evaluated with water suspensions of PS NPs with various certified diameters ranging from 800 to 60 nm, as well as other NPs with different polymer type and size distribution such as PMMA (300 nm), PP (180 nm), PET (100 nm), and PE (450 nm), serving as fit-for-purpose representative test materials. The acquired spectra demonstrated a high signal-to-noise ratio, allowing clear identification of many characteristic polymeric peaks, also for NPs smaller than 200 nm. The high quality of Raman spectra enabled a deeper investigation into the differences between the NPs and the bulk plastic polymers used as control, including the identification of potential oxidative states of the NPs. Finally, NPs dispersed in commercial brand drinking water were successfully detected by the DEP-Raman system, demonstrating the potential of this innovative methodology for detection and chemical characterization of NPs in real-world matrices.

Materials and methods

Particles and chemicals

NIST spherical PS nanoparticles suspended in MilliQ water with a diameter of 60 nm (certified mean diameter: 60 nm ± 4 nm, k = 2; standard deviation: 5.1 nm; coefficient of variation: 2.5%; hydrodynamic diameter: 58–68 nm; density: 1.05 g/cm^3; index of refraction: 1.59 at 589 nm), 200 nm (certified mean diameter: 202 nm ± 4 nm, k = 2; standard deviation: 10.5 nm; coefficient of variation: 17.5%; hydrodynamic diameter: 199–210 nm; density: 1.05 g/cm^3; index of refraction: 1.59 at 589 nm), and 500 nm (certified mean diameter: 510 nm ± 7 nm, k = 2; standard deviation: 9.2 nm; coefficient of variation: 1.8%; density: 1.05 g/cm^3; index of refraction: 1.59 at 589 nm) were purchased from Duke standards. PS particles suspended in water with a diameter of 800 nm (mean particle size: 0.8 µm) were purchased from Sigma Aldrich. PS particles suspended in water with a diameter of 100 nm (coefficient of variation: < 3%) were obtained from Alfa Test. PMMA particles suspended in water with a diameter of 300 nm (coefficient of variation: < 3%) were obtained from Alfa Test. PP and PE particles were produced as previously reported by Hildebrandt et al. and provided by Bundesanstalt für Materialforschung undprüfung (Berlin, Germany) [32]. PET particles were produced as previously reported by Robles-Martín et al. and provided by Consejo Superior de Investigaciones Científicas (Madrid, Spain) [33]. Ultrapure water was obtained by MilliQ QI-7000 purification system (Merck Millipore, Germany). Phosphate Buffer Saline (PBS) was purchased by PanReac AppliChem (Darmstadt, Germany). Commercial brand bottled drinking water purchased from a local supermarket as a representative real-world matrix.

Nanoplastics suspension preparation

NPs suspensions were prepared with a concentration of 40 µg/mL. The prepared NPs suspensions' labels with all the information related to the starting material are

Table 1 Labels indicating the polymer type and approximate diameter of the NPs used in this study, initial concentration (C_i) of the as received sample, final concentration (C_f) after dilution in filtered MilliQ water for DLS and DEP-Raman characterization, hydrodynamic diameter (D_h) and polydispersity index (PDI) measured by DLS. Both D_h and PDI are expressed as average ± standard deviation

Label	Supplier	C_i (mg/mL)	C_f (mg/mL)	$D_h \pm$ s.d (nm)	PDI ± s.d
PS 800	Sigma Aldrich	100	0.04	813 ± 10	0.05 ± 0.04
PS 500	Duke standards	10	0.04	535.8 ± 6.2	0.07 ± 0.05
PS 200	Duke standards	10	0.04	215.9 ± 1.5	0.038 ± 0.019
PS 100	Alfa Test	10	0.04	114.6 ± 0.9	0.017 ± 0.009
PS 60	Duke standards	10	0.04	70.9 ± 0.6	0.017 ± 0.009
PMMA 300	Alfa Test	10	0.04	362 ± 5	0.025 ± 0.017
PP 180	BAM	0.04	0.04	180 ± 4	0.07 ± 0.03
PET 100	CSIC	4.9	0.04	98 ± 3	0.18 ± 0.06
PE 450	BAM	0.08	0.04	459 ± 44	0.33 ± 0.09

reported in Table 1. PS, PMMA, PET, and PE suspensions were diluted in ultrapure water that was previously filtrated with cellulose nitrate membrane filters (pore size: 0.1 µm). Then, they were sonicated in an ultrasound bath for 15 min to prevent the formation of agglomerates in the suspension. PP was used at its native concentration, approximately 40 µg/mL [32]. PS 200, PP 180, and PET 100 suspensions were spiked in bottled water with 1:1 ratio, without any further matrix treatment or preparation, having a final concentration of NPs in the medium of 20 µg/mL.

Dynamic light scattering (DLS)

Z-average and polydispersity index (PDI) of NPs suspensions were evaluated by DLS using a ZETASIZER Ultra (Malvern Panalytical, United Kingdom). Back-scattering (angle 173°) was used for the measurement. 5 runs per measurement were conducted on each sample. The operating temperature was maintained at 25 °C. The average hydrodynamic diameter (D_h) and PDI were obtained from the correlation function fitted according to ISO 22412:2017 [34].

Scanning electron microscopy (SEM)

SEM was used to investigate the morphology and the size of PP 180, PE 450, and PET 100. In detail, a Supra 40 SEM (Zeiss, Oberkochen, Germany) equipped with a Schottky-field emitter, a secondary electron InLens detector, and a dedicated sample holder which enables transmission imaging (TSEM) was used for the analysis of PP 180 and PE 450. The particles were prepared by drop-casting 2–6 µL of the suspension on transmission electron microscope (TEM) grids, previously ozonated, and then dried in a desiccator. The beam voltage was 10 kV, and the working distance was 4.8 mm. Furthermore, a FEI Nova NanoSEM 230field emission scanning electron microscope was used to acquire images for PET 100. The dried drops of the sample were gold-sputtered for 25 s in a Leika EM ACE200 coating system at 30 mA and 0.5 bar Ar.

Dielectrophoresis and Raman spectroscopy

For characterization by coupling DEP and Raman spectroscopy, 50 µL of each NPs' suspension were mixed with 5 µL of 10% PBS solution. Volumes of 5 µL of these suspensions were injected into a dielectrophoretic cell manufactured in our laboratories [23]. The electrical field in the DEP cell was induced by a sinusoidal voltage of 5 V peak-to-peak at a frequency of 1 MHz obtained by a Hewlett-Packard 33120a (United States) function generator, resulting in negative DEP and net forces on the samples directed towards the center of the cell, where the confocal volume of a Raman Imaging microscope (DXRxi, Thermo Scientific, United States) was located. NPs accumulation time before Raman spectra acquisition was 30 s. Spectra were acquired with a 60 ×water immersion objective (N.A. =1.1) by using an excitation wavelength at 532 nm, a laser power of 20 mW, an exposure time of 1 s for 60 scans (1 min total per spectrum), and a spectrograph confocal pinhole aperture of 50 µm in diameter. The dispersive Raman system has 5 cm^{-1} spectral resolution and a spectral range of 500–3100 cm^{-1}. A scheme of the method is reported in Fig. 1.

Results and discussion

NPs size, stability and morphology: DLS and SEM

The hydrodynamic diameter (D_h) and polydispersity index (PDI) of the NPs suspensions obtained by DLS are reported in Table 1. The D_h of the diluted suspensions made with commercial PS 800, PS 500, PS 200, PS 100, and PS 60 polystyrene samples correspond with the reported diameter. On the other hand, as certified reference materials their expected monodispersity is confirmed by PDI accordingly with the ISO 22412:2017 [34], where the PDI is less than 0.07 for a monodisperse test sample of spherical particles. This means that the dilution in MilliQ water does not affect the size distribution of the particles in a relevant way. The same effects are observed for commercial PMMA 300. However, suspensions with PET 100, PP 180 (non-diluted) and PE 450 present a D_h of approximately 98 nm, 180 nm and 458

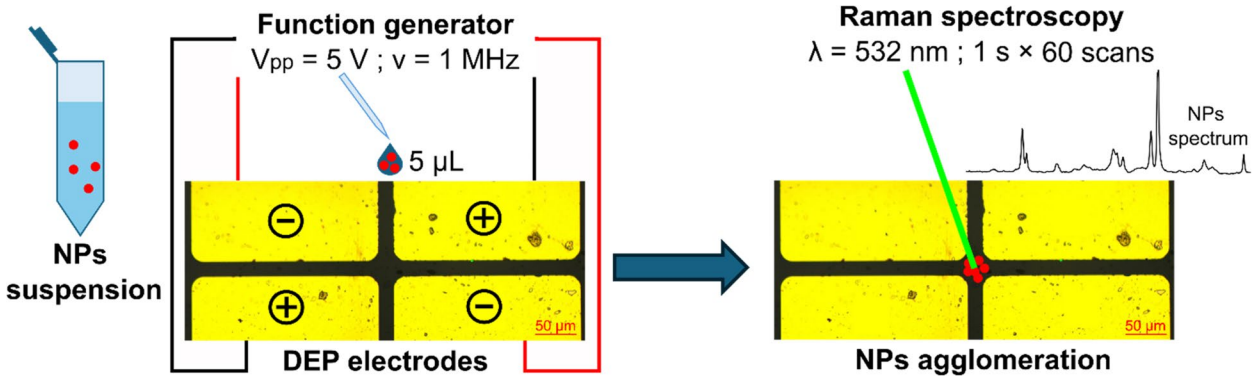

Fig. 1 Schematic representation of DEP-Raman system for NPs chemical identification: NPs suspension is injected into the DEP cell, which is connected to a function generator by two wires (red and black) to induce a specific voltage, and finally the agglomeration of NPs is obtained, where the laser (green wavelength) is pointed, allowing the chemical identification of the species

nm, respectively, well in agreement with the values provided by the supplier after manufacturing. PDI values indicated polydisperse suspensions according with the ISO 22412:2017 [34].

The morphology as size and shape of PP 180, PE 450 and PET 100 was investigated by SEM, and representative micrographs are shown in Fig. 2. The observed dimensions are in the range of those found by the DLS measurements (see Table 1). While PET 100, obtained by dissolution and reprecipitation in water, have a regular spherical shape, both PP 180 and PE 450, obtained by mechanical fractionation, have irregular shapes, with a fragment-like appearance and complex (highly non-spherical and rough) morphology, making these samples more representatives for real NPs that could be found in food or environmental matrices.

Identification of NPs in MilliQ and bottled water: DEP-Raman

DEP-Raman system allowed the chemical identification of the most representative NPs species in terms of types of polymers, with high signal-to-noise ratio Raman spectra. When the voltage is not applied the Raman spectrum of the medium is acquired both for ultrapure water and bottled water, as can be noticed in Figure S1 (See Supporting information). Then, the application of the specific voltage leads to the activation of negative DEP phenomenon with the consequential concentration of injected NPs at the center of the electrode, where the laser of the Raman is spotted.

The Raman spectra of PS NPs dispersed in MilliQ water obtained with DEP-Raman system in the spectral range between 3000 cm^{-1} and 600 cm^{-1} are reported in Fig. 3, alongside the spectrum of a macroscopic PS sample (bulk) used as reference. The position in Raman shift of the characteristic PS peaks, in the regions of the aromatic (3100–3000 cm^{-1}) and the aliphatic (3000–2800 cm^{-1}) C-H stretching, and their assignments are reported in Table S1 (See Supporting Information) [35, 36]. While the spectra of PS 800, PS 500, PS 200, and PS 100 perfectly correspond to that of PS bulk, PS 60 spectrum presents some differences that are highlighted in blue in Fig. 3. In particular, the peak at 2937 cm^{-1} in the aliphatic C-H stretching region is strong in intensity, whereas the peaks at 2905 cm^{-1} and 2849 cm^{-1} of PS bulk are shifted and less strong in intensity in PS 60. In addition, the small peaks of PS bulk at 1741 cm^{-1} and 1731 cm^{-1} are more evident in PS 60, but not clearly appreciated in the

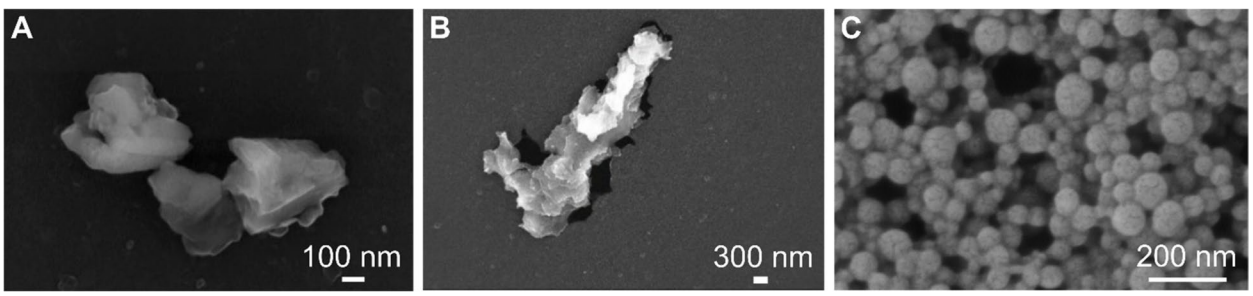

Fig. 2 Representative SEM images of (**A**) PP 180, (**B**) PE 450, and (**C**) PET 100

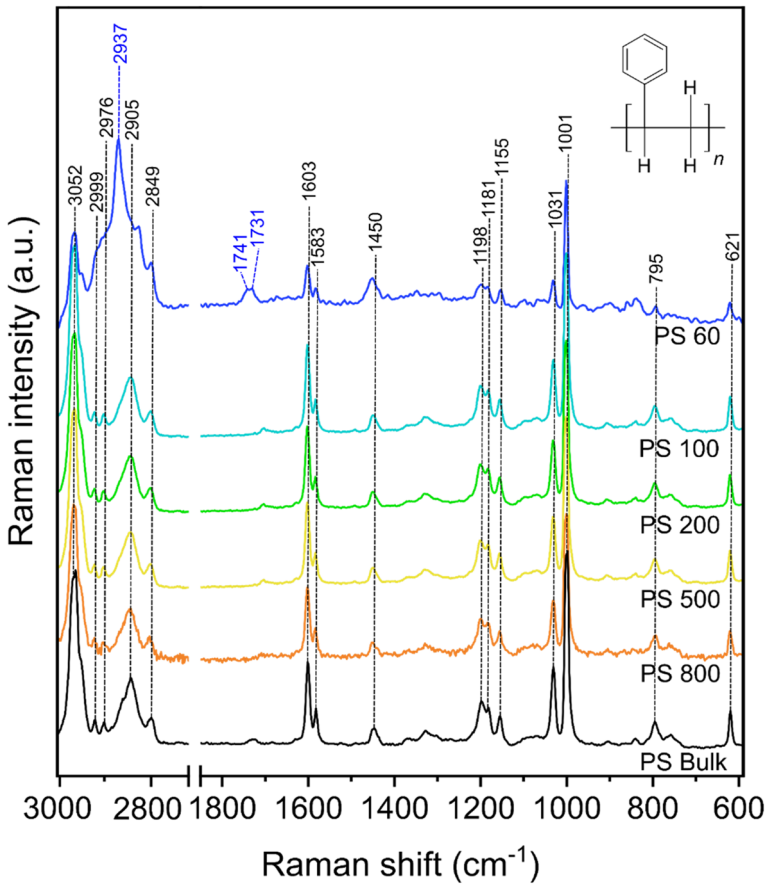

Fig. 3 Raman spectra of (from the bottom) PS bulk, as reference, with Raman shifts corresponding to the peak positions marked in black, as well as of PS 800, PS 500, PS 200, PS 100, and PS 60. The varying peak positions of PS 60 are marked in blue. The spectra are overlaid vertically for better comparison

other PS NPs: they could be assigned to the stretching of the carbonyl group (C = O) that might be formed due to photo-oxidation of PS [37].

The Fig. 4 compares the Raman spectra of the other NPs suspended in MilliQ water obtained with the DEP-Raman system, and their plastic bulk counterparts: the bulk peak positions expressed in Raman shift are marked in black, and their correspondent assignments are reported in Table S2 (See Supporting Information) for PMMA, in Table 2 for PP, in Table 3 for PET, and in Table 4 for PE. All the peaks of PMMA 300 (Fig. 4A) perfectly correspond to the spectrum of the bulk sample, apart from one peak that shifted from 2843 cm^{-1} in the bulk to 2821 cm^{-1} in PMMA 300, assigned to the symmetric stretching of CH_3 that appears in the spectral range between 3000 cm^{-1} and 2840 cm^{-1} in methyl esters. (Tables 3 and 4).

More differences were observed between PP 180 and PP bulk, not only in the peak positions but also in their relative intensities (Fig. 4B). In the PP 180 spectrum, the peak at 2840 cm^{-1}, assigned to the symmetric stretching of CH_2, shifted to 2848 cm^{-1}. In addition, two peaks appear at 1650 cm^{-1} and 1605 cm^{-1}, assigned to the stretching of the carbonyl group (C = O) formed due to possible oxidation of PP 180 during its preparation procedure, since PP granules were soaked in acetone and then dispersed [32]. The fingerprint region also presents significant variations: the peaks of PP bulk at 1436 cm^{-1}, 1254 cm^{-1}, 1219 cm^{-1}, 1168 cm^{-1}, 1153 cm^{-1}, and 940 cm^{-1} shifted to 1445 cm^{-1}, 1277 cm^{-1}, 1202 cm^{-1}, 1157 cm^{-1}, 1127 cm^{-1}, and 929 cm^{-1} in PP 180, respectively. Also, the two evident peaks in PP bulk at 842 cm^{-1} and 810 cm^{-1} disappeared in PP 180, with the formation of an intermediate peak at 830 cm^{-1}.

In case of PET 100 (Fig. 4C), the relative intensities also vary due to possible changes in the crystallinity of the polymer [39], whereas the peak positions are essentially the same as in the PET bulk, with slightly changes as for the peak at 1187 cm^{-1}, assigned to the stretching of the aromatic C-H in-plane and of C–C, that appears at 1176 cm^{-1} in PET 100.

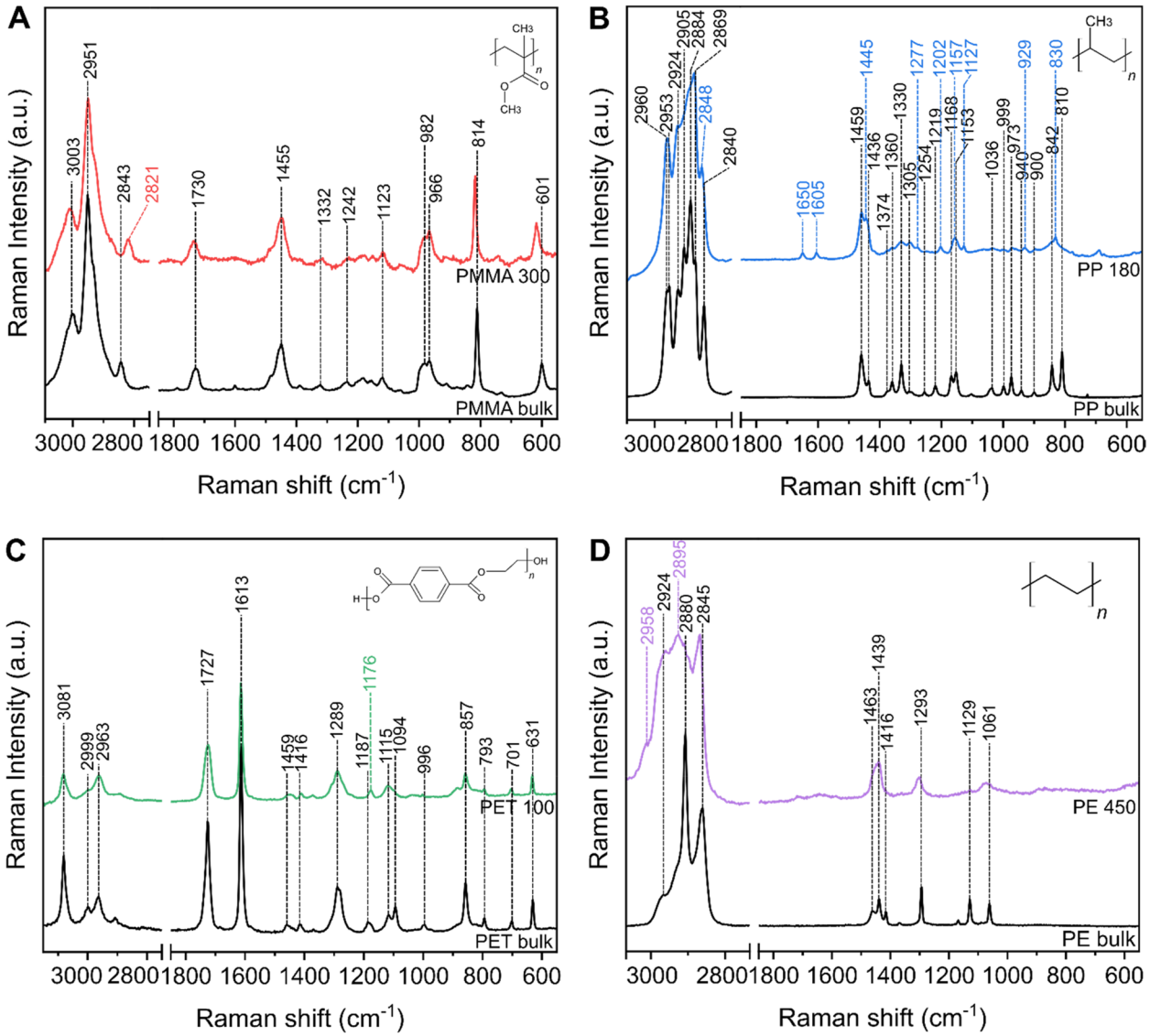

Fig. 4 Raman spectra of NPs suspended in MilliQ compared to their bulk counterparts (**A**) PMMA 300, (**B**) PP 180, (**C**) PET 100, (**D**) PE 450. The spectra are overlaid vertically for better comparison

On the contrary, in Fig. 4D several differences can be noticed between PE bulk and PE 450. In particular, the peak at 2958 cm^{-1} of PE 450 does not correspond to the peak in PE bulk and it was assigned to the asymmetric stretching of CH_3 typical of the alkanes in the range between 3000 cm^{-1} and 2940 cm^{-1}. Furthermore, the peak at 2880 cm^{-1} in PE bulk shifts to 2895 cm^{-1} in PE 450. In the fingerprint region, the sharp and well-defined peaks of bulk PE give place to broad bands in PE 450. In particular, the peaks at 1293 cm^{-1} and 1080 cm^{-1} are related in the literature to amorphous PE, whereas the peaks at 1416 cm^{-1}, 1129 cm^{-1} and 1061 cm^{-1}, which are indicative of high crystallinity in PE bulk [41], disappear in PE 450. All these changes could be related to the procedure used to make PE 450 that changed the polymeric conformation with consequential different exposure of molecules and bonds [32].

Therefore, Raman spectroscopy enabled by DEP overcomes the spatial resolution limitations of the traditional Raman spectroscopy, allowing the chemical identification of NPs across a wide size range, from 800 to 60 nm, including not certified reference materials that are more representative of real samples in terms of shape and size distribution. Moreover, the high signal-to-noise ratio of NPs Raman spectra allows to highlight potential alterations compared to the corresponding bulk plastic, which

Table 2 Raman shifts (cm^{-1}) and relative assignments of PP bulk [38]

Raman shift (cm^{-1})	Assignment
2960	ν_a (CH_3)
2953	ν_a (CH_3)
2924	ν_a (CH_2)
2905	ν_a (CH_2)
2884	ν_s (CH_3)
2869	ν_s (CH_2)
2840	ν_s (CH_2)
1459	δ_a (CH_3), δ (CH_2)
1436	δ_a (CH_3)
1374	in plane ρ (CH)
1360	δ_s (CH_3), δ (CH_2)
1330	δ (CH), τ (CH_2)
1305	w (CH_2), τ (CH_2)
1254	δ (CH), τ (CH_2), ρ (CH_3)
1219	τ (CH_2), δ (CH), ν (CC_b)
1168	ν (CC_b), δ (CH_3), ρ (CH_3)
1153	ν (CC_b), ν (C-CH_3), δ (CH_3), ρ (CH_3)
1036	ν (C-CH_3), ν (CC_b), δ (CH)
999	ρ (CH_3), δ (CH), w (CH_2)
973	ρ (CH_3), ν (CC_b)
940	ρ (CH_3), ν (CC_b)
900	ρ (CH_3), ρ (CH_2), δ (CH)
842	ρ (CH_2), ν (CC_b), ν (C-CH_3), ρ(CH_3)
810	ρ (CH_2), ν (CC_b), ν (C-CH_3)

Table 3 Raman shifts (cm-1) and relative assignments of PET bulk [40]

Raman shift (cm^{-1})	Assignment
3081	Aromatic ν (C – H)
2999	ν_a (CH_3)
2963	Methylene groups adjacent to oxygen atoms
1727	ν_s (C = O)
1613	Ring mode 8a (in Wilson's notation)
1459	δ (CH_2), δ (OCH)
1416	δ (CCH), δ (OCH)
1289	ν (C – O – O)
1187	Ring in plane C–H bond and C–C stretch
1115	Ester C(O)–O and ethylene glycol C–C bonds
1094	ν (C – O)
996	ν (C – C)
857	C – C breathing mode
793	CH out-of-plane, ring
701	C–C-C out-of-plane, ring
631	C–C-C in-plane bend, ring

Table 4 Raman shifts (cm^{-1}) and relative assignments of PE bulk [41]

Raman shift (cm^{-1})	Assignments
2924	ν_a (CH_2)
2880	ν_s (CH_3)
2845	ν_s (CH_2)
1463	δ (CH_2)
1439	δ (CH_2)
1416	δ (CH_2)
1293	τ (CH_2)
1129	ν_s (C – C)
1061	ν_a (C – C)

reflect structural and/or chemical changes such as amorphization, surface oxidation and/or chemical degradation caused by the NPs preparation method or storage conditions. The presented DEP-Raman system is particularly valuable for monitoring polymer degradation processes for small particles, such as NPs, as it provides detailed information about the chemical bonds and molecular vibrations both within and on the surface of the material. Understanding these modifications is crucial for accurately assessing the risks associated with the sample, therefore this DEP-Raman system could be considered in NPs risk assessment frameworks. Several key changes can be observed in the Raman spectra. Shifts in Raman peaks, such as those associated with aromatic rings or functional groups, may indicate chemical bond breaking or rearrangement, as seen in PP 180. Changes in peak intensity, associated to specific bonds due to the breakdown or buildup of certain functional groups or molecular chains, (e.g. the intensity of peaks associated with carbon–carbon bonds may decrease as the polymer chain shortens or breaks), mainly occurred for PP 180 and PE 450. The emergence of new peaks, because of the formation of new functional groups, which are often carbonyl groups related to aldehydes or carboxylic acid, correspondent to oxidative status of the material due to environmental factors such as heating, UV light, or mechanical stress. In this study, new peaks were clearly observed in PS 60 and PP 180 in the region between 1700 cm^{-1} and 1600 cm^{-1}. Finally, polymer degradation often leads to increased disorder within the molecular structure, resulting in broader, less sharp peaks, as well as changes in the relative intensity, indicating a loss of regularity in the molecular structure of the polymer, as mainly occurred for PP 180 and PE 450.

In addition, the DEP-Raman system enabled the identification of NPs suspended in MilliQ water at concentrations as low as 40 μg/mL. For instance, considering the

minimal detectable concentration of 200 µg/mL detected on PS 200 with Raman enabled by optical tweezer reported by Schwaferts et al. [19], the DEP-Raman system is able to significantly lower the detectable concentration. Furthermore, the signal-to-noise ratio of the spectra of NPs with size smaller than 100 nm was higher than results reported in the state of the art regarding Raman tweezer technique [20], as well as a complete chemical information in the entire spectral range (500–3100 cm^{-1}) for each analyzed material. Same considerations can be done for NPs spotted on silicon wafers: few characteristic peaks are visible for the investigated polymers due to the low signal-to-noise ratio of the presented spectra [16]. A good quality of the Raman spectra leads to a better classification of the spectra when compared with standard libraries, therefore more affordable data and less false positive, as suggested by Xu et al. [42]. Finally, DEP-Raman system does not require a large sample volume and a complex preparation step, as few microliters of the NPs suspension are directly injected into the DEP cell. Therefore, the possibility to analyze directly suspended NPs that are demonstrated to be homogeneously dispersed into the water matrix by DLS measurements, makes the presented method more valuable in terms of reproducibility and reliability.

Therefore, DEP-Raman system can be considered a valuable method to detect and deeply characterize NPs in aqueous matrices. Considering these successful results, the DEP-Raman system was also employed to identify PET 100, PP 180, and PS 200 after spiking them into a commercial brand of drinking water, with their spectra reported in Fig. 5. PS 200 was selected as a control sample, whereas PP 180 and PET 100 were chosen as they are more representative in terms of type, size and shape for real NPs, and among the most used polymers in food packaging. Interestingly, high-quality Raman spectra were obtained for all NPs spiked into bottled water, showing the same characteristic peaks as those observed for the corresponding NPs suspensions in Milli-Q water. This applicative study revealed that the DEP-Raman system can be used for the identification of NPs in a real matrix at concentrations as low as 20 µg/mL, while still producing Raman spectra with high signal-to-noise ratio. In addition, this application revealed another important result related to the sample preparation step: using NP suspensions directly in the DEP-Raman system is not

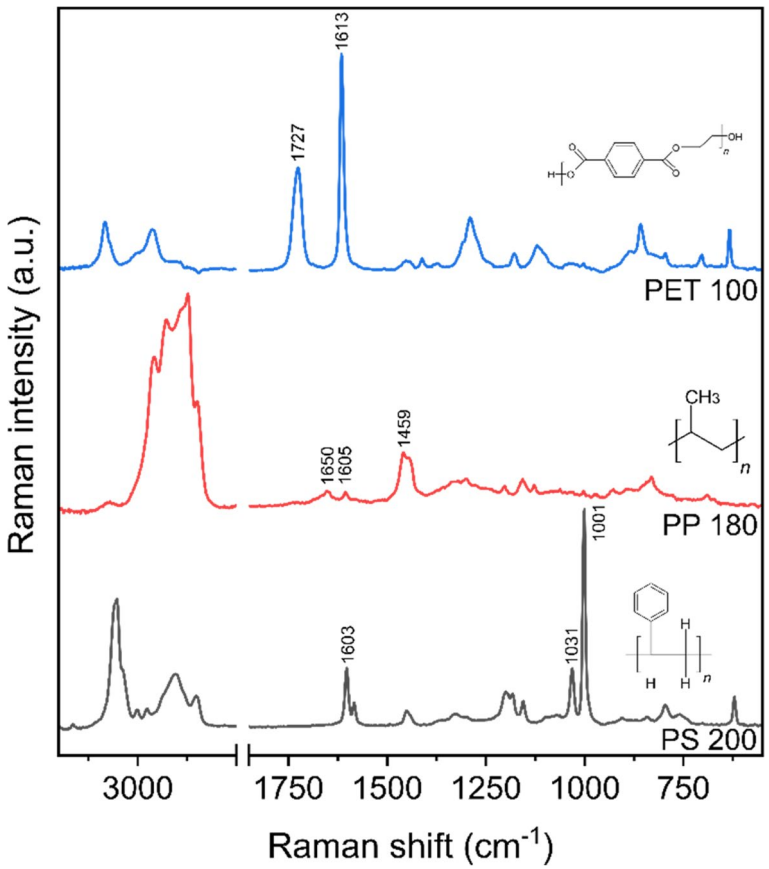

Fig. 5 Raman spectra of PS 200, PP 180, and PET 100 spiked in bottled water. The spectra are overlaid vertically for better comparison

only practically convenient but also minimizes interference from medium-soluble components, such as salts, which remain dissolved and do not affect the reliability of Raman spectroscopy identification. Of course, increasing the complexity of the analyzed water, such as tap water or environmental water, some additional steps must be taken in consideration in the sample preparation procedure: for instance, the removal of bigger particles and compounds that can disturb the analysis should be done by performing a cascade filtration or a specific matrix treatment (e.g. enzymatic or chemical digestion). Or, since the number of NPs in real matrices is considerably smaller than the number of contaminants, pre-concentrating or enriching the sample should be considered.

Conclusions

This work demonstrates the feasibility of Raman spectroscopy enabled by DEP for the chemical identification of NPs suspensions both in MilliQ and bottled drinking water. This method overcomes the spatial resolution limitations of Raman spectroscopy by locally increasing NP concentrations, with DEP forces accumulating them to fill the Raman confocal volume, enabling their detection and identification for more reliable analysis. In this study, even if a broader range of sizes including MPs could be analyzed by DEP-Raman system, we decided to focus much more on the NPs range, since methods for their chemical identification are still lacking. In addition to allow the direct analysis of NPs in their suspension medium without complex sample preparation, the high signal-to-noise ratio of the obtained Raman spectra highlights the feasibility of this DEP-Raman system for the identification of NPs comprised in a size range between 800 and 60 nm. This includes not only certified reference materials but also materials more representative of real-world NPs in terms of shape, size distribution and morphology, as demonstrated by SEM images. In addition, good quality spectra allow an in-depth analysis in comparison with bulk polymers as reference, understanding possible oxidative status or structural and chemical changes that may occur during particle degradation processes, as demonstrated, for instance, for PP 180. Indeed, the identification of early-stage degradation is essential for evaluating the durability and environmental impact of polymers, especially in the context of materials such as plastics that are subject to long-term exposure to environmental conditions. Furthermore, the applicative study in bottled drinking water fixes the detectable concentration of NPs in suspension at nearly 20 µg/mL, making this method a good alternative to similar methods for identification of NPs. Further optimization of the operating conditions, along with on-line/off-line integration with other orthogonal methodologies, such as fractionation tools (e.g. asymmetrical flow filed-flow fractionation), dimensional techniques (e.g. DLS), and number-based concentration techniques (e.g. nanoparticle tracking analysis), can provide a more comprehensive physico-chemical characterization of heterogeneous NPs and extend the applicability of the DEP-Raman system to other relevant media. Given the recent release of the Delegated Decision (EU) 2024/1441 for monitoring MPs in drinking water and the expected future focus on NPs, this innovative method offers a promising solution to bridge existing gaps in the detection and identification of NPs in real-world matrices, a field that remains in its early stages.

Supplementary Information

The online version contains supplementary material available at https://doi.org/10.1186/s43591-025-00131-y.

Supplementary Material 1

Acknowledgements
The authors thank Dr. Vasile-Dan Hodoroaba (Bundesanstalt für Materialforschung und-prüfung (BAM), 12205, Berlin, Germany) for review and editing the original draft.

Authors' contribution
Marta Fadda: Conceptualization, Methodology, Experimental Execution, Investigation, Writing—original draft. Alessio Sacco: Methodology, Experimental Execution, Writing – review & editing. Korinna Altmann: Writing – review & editing, Funding. Dmitri Ciornii: Experimental Execution – SEM images. Frank Milczewski: Experimental Execution – PP 180 preparation. Miguel A. Bañares, Raquel Portela: Experimental Execution – PET 100 preparation, Writing – review & editing, Funding. Andrea Mario Giovannozzi: Writing – review & editing, Supervision, Funding. Andrea Mario Rossi: Writing – review & editing, Supervision, Funding.

Funding
-METROFOOD-IT project has received funding from the European Union -NextGenerationEU, PNRR—Mission 4 "Education and Research" Component 2: from research to business, Investment 3.1: Fund for the realisation of an integrated system of research and innovation infrastructures—IR0000033 (D.M. Prot. n.120 del 21/06/2022).
-The project 21GRD07 PlasticTrace (Funder ID: https://doi.org/10.13039/100019599) has received funding from the European Partnership on Metrology, co-financed from the European Union's Horizon Europe Research and Innovation Programme and by the Participating States."
-The European Commission for funding the H2020 Project "Plastics Fate and Effects in the human body" (PlasticsFate) under Grant Agreement no. 95921
-This publication has been funded by the Italian Ministry of University and Research (MUR) in the framework of the continuing-nature project "NEXT-GENERATION METROLOGY", under the allocation of the Ordinary Fund for research institutions (FOE) 2023 (Ministry Decree n. 789/2023).

Data availability
Sequence data that support the findings of this study have been deposited in Zenodo with https://doi.org/10.5281/zenodo.14762447.

Declarations

Competing interests
The authors declare no competing interests.

Received: 29 January 2025 Accepted: 19 May 2025
Published online: 04 June 2025

References

1. Sangkham S, et al. A review on microplastics and nanoplastics in the environment: Their occurrence, exposure routes, toxic studies, and potential effects on human health. Mar Pollut Bull. 2022;181: 113832.
2. Sana SS, Dogiparthi LK, Gangadhar L, Chakravorty A, Abhishek N. Effects of microplastics and nanoplastics on marine environment and human health. Environ Sci Pollut Res. 2020;27:44743–56.
3. Lehner R, Weder C, Petri-Fink A, Rothen-Rutishauser B. Emergence of nanoplastic in the environment and possible impact on human health. Environ Sci Technol. 2019;53(4):1748–65.
4. 'ISO/TR 21960:2020(en) Plastics — Environmental aspects — State of knowledge and methodologies'. 2020. [Online]. Available: https://www.iso.org/obp/ui/en/#iso:std:iso:tr:21960:ed-1:v1:en
5. Yee MS-L, et al. Impact of microplastics and nanoplastics on human health. Nanomaterials. 2021;11(2):496.
6. Barnes DK, Galgani F, Thompson RC, Barlaz M. Accumulation and fragmentation of plastic debris in global environments. Philos Trans R Soc B Biol Sci. 2009;364(1526):1985–98.
7. Ivleva NP. Chemical analysis of microplastics and nanoplastics: challenges, advanced methods, and perspectives. Chem Rev. 2021;121(19):11886–936.
8. SAPEA (Science advice for policy by European academies). A scientific perspective on microplastics in nature and society. Berlin: SAPEA; 2019.
9. Bressot C, Meunier L, Dutouquet C. Particle emissions study from tire sample with nano-silver tracer from different steps of its life cycle. A new approach to trace emissions of tire microparticles. Sci Total Environ. 2025;959: 178221.
10. Geng Y, Zhang Z, Zhou W, Shao X, Li Z, Zhou Y. Individual exposure to microplastics through the inhalation route: comparison of microplastics in inhaled indoor aerosol and exhaled breath air. Environ Sci Technol Lett. 2023;10(6):464–70.
11. Domenech J, Hernández A, Rubio L, Marcos R, Cortés C. Interactions of polystyrene nanoplastics with in vitro models of the human intestinal barrier. Arch Toxicol. 2020;94:2997–3012.
12. Mitrano DM, Beltzung A, Frehland S, Schmiedgruber M, Cingolani A, Schmidt F. Synthesis of metal-doped nanoplastics and their utility to investigate fate and behaviour in complex environmental systems. Nat Nanotechnol. 2019;14(4):362–8.
13. Hong J, Lee B, Park C, Kim Y. A colorimetric detection of polystyrene nanoplastics with gold nanoparticles in the aqueous phase. Sci Total Environ. 2022;850: 158058.
14. Gigault J, et al. Nanoplastics are neither microplastics nor engineered nanoparticles. Nat Nanotechnol. 2021;16(5):501–7.
15. Huber MJ, et al. Physicochemical characterization and quantification of nanoplastics: applicability, limitations and complementarity of batch and fractionation methods. Anal Bioanal Chem. 2023;415(15):3007–31.
16. Caldwell J, et al. Detection of submicron-and nanoplastics spiked in environmental fresh-and saltwater with Raman spectroscopy. Mar Pollut Bull. 2024;203: 116468.
17. Schmidt R, et al. Correlative SEM-Raman microscopy to reveal nanoplastics in complex environments. Micron. 2021;144: 103034.
18. Sobhani Z, Zhang X, Gibson C, Naidu R, Megharaj M, Fang C. Identification and visualisation of microplastics/nanoplastics by Raman imaging (i): Down to 100 nm. Water Res. 2020;174: 115658.
19. Schwaferts C, et al. Nanoplastic analysis by online coupling of Raman microscopy and field-flow fractionation enabled by optical tweezers. Anal Chem. 2020;92(8):5813–20.
20. Gillibert R, et al. Raman tweezers for small microplastics and nanoplastics identification in seawater. Environ Sci Technol. 2019;53(15):9003–13.
21. Lv L, et al. In situ surface-enhanced Raman spectroscopy for detecting microplastics and nanoplastics in aquatic environments. Sci Total Environ. 2020;728: 138449.
22. Zhou X-X, Liu R, Hao L-T, Liu J-F. Identification of polystyrene nanoplastics using surface enhanced Raman spectroscopy. Talanta. 2021;221: 121552.
23. Barzan G, et al. New frontiers against antibiotic resistance: A Raman-based approach for rapid detection of bacterial susceptibility and biocide-induced antibiotic cross-tolerance. Sens Actuators B Chem. 2020;309: 127774.
24. Sacco A, et al. Raman-dielectrophoresis goes viral: towards a rapid and label-free platform for plant virus characterization. Front Microbiol. 2023;14:1292461.
25. Barzan G, et al. Molecular aspects of the interaction with gram-negative and gram-positive bacteria of hydrothermal carbon nanoparticles associated with Bac8c2, 5Leu antimicrobial peptide. ACS Omega. 2022;7(19):16402–13.
26. Khoshmanesh K, Nahavandi S, Baratchi S, Mitchell A, Kalantar-zadeh K. Dielectrophoretic platforms for bio-microfluidic systems. Biosens Bioelectron. 2011;26(5):1800–14.
27. Bu S, Sonker M, Koh D, Ros A. On the behavior of sub-micrometer polystyrene particles subjected to AC insulator-based dielectrophoresis. Electrophoresis. 2024;45:1860–73.
28. Beech JP, Keim K, Ho BD, Guiducci C, Tegenfeldt JO. Active posts in deterministic lateral displacement devices. Adv Mater Technol. 2019;4(9):1900339.
29. Sacco A, et al. Characterization of plant pathogenic bacteria at subspecies level using a dielectrophoresis device combined with Raman spectroscopy. Biosens Bioelectron X. 2025;23: 100595.
30. Ulrich-Christian S, et al. Combined Dielectrophoresis–Raman Setup for the Classification of Pathogens Recovered from the Urinary Tract. Electrophoresis. 2013;34(7):998–1004.
31. Chrimes AF, et al. Dielectrophoresis–Raman spectroscopy system for analysing suspended nanoparticles. Lab Chip. 2011;11(5):921–8.
32. Hildebrandt J, Thünemann AF. Aqueous dispersions of polypropylene: toward reference materials for characterizing nanoplastics. Macromol Rapid Commun. 2023;44(6):2200874.
33. Robles-Martín A, et al. Sub-micro-and nano-sized polyethylene terephthalate deconstruction with engineered protein nanopores. Nat Catal. 2023;6(12):1174–85.
34. 'ISO 22412:2017 Particle size analysis — Dynamic light scattering (DLS)'. Feb. 2017. [Online]. Available: https://www.iso.org/obp/ui/en/#iso:std:iso:22412:ed-2:v1:en
35. Fan Y, Cornelius CJ. Raman spectroscopic and gas transport study of a pentablock ionomer complexed with metal ions and its relationship to physical properties. J Mater Sci. 2013;48:1153–61.
36. Mazilu M, Luca ACD, Riches A, Herrington CS, Dholakia K. Optimal algorithm for fluorescence suppression of modulated Raman spectroscopy. Opt Express. 2010;18(11):11382–95.
37. Lucki J, Rånby B. Photo-oxidation of polystyrene—Part 2: Formation of carbonyl groups in photo-oxidised polystyrene. Polym Degrad Stab. 1979;1(3):165–79.
38. Andreassen E. Infrared and Raman spectroscopy of polypropylene. Polypropyl. AZ Ref. 1999:320–8.
39. Tamargo A, et al. PET microplastics affect human gut microbiota communities during simulated gastrointestinal digestion, first evidence of plausible polymer biodegradation during human digestion. Sci Rep. 2022;12(1):528.
40. Rebollar E, et al. Physicochemical modifications accompanying UV laser induced surface structures on poly (ethylene terephthalate) and their effect on adhesion of mesenchymal cells. Phys Chem Chem Phys. 2014;16(33):17551–9.
41. Fischer J, Wallner GM, Pieber A. Spectroscopical investigation of ski base materials. Macromol Symp. 2008;265:28–36.
42. Xu J-L, Wright S, Rauert C, Thomas KV. Are microplastics bad for your health? More rigorous science is needed. Nature. 2025;639(8054):300–2.

Publisher's Note